Soft Matter

PAPER

View Article Online
View Journal

Cite this: DOI: 10.1039/c6sm00606j

Elasticity of fibrous networks under uniaxial prestress

Mahsa Vahabi,[a] Abhinav Sharma,[a] Albert James Licup,[a] Anne S. G. van Oosten,[b] Peter A. Galie,[b] Paul A. Janmey[b] and Fred C. MacKintosh*[a]

Received 10th March 2016,
Accepted 5th May 2016

DOI: 10.1039/c6sm00606j

www.rsc.org/softmatter

We present theoretical and experimental studies of the elastic response of fibrous networks subjected to uniaxial strain. Uniaxial compression or extension is applied to extracellular networks of fibrin and collagen using a shear rheometer with free water in/outflow. Both uniaxial stress and the network shear modulus are measured. Prior work [van Oosten, *et al.*, *Sci. Rep.*, 2015, **6**, 19270] has shown softening/stiffening of these networks under compression/extension, together with a nonlinear response to shear, but the origin of such behaviour remains poorly understood. Here, we study how uniaxial strain influences the nonlinear mechanics of fibrous networks. Using a computational network model with bendable and stretchable fibres, we show that the softening/stiffening behaviour can be understood for fixed lateral boundaries in 2D and 3D networks with comparable average connectivities to the experimental extracellular networks. Moreover, we show that the onset of stiffening depends strongly on the imposed uniaxial strain. Our study highlights the importance of both uniaxial strain and boundary conditions in determining the mechanical response of hydrogels.

1 Introduction

Proteins, essential molecules of living organisms, can be found in the form of fibrous networks both inside and outside the cells.[1–7] The cytoskeleton, blood clots and extracellular matrices of tissues all consist of fibrous protein networks. The mechanics of these systems depend not only on the elastic properties of the individual fibres but also on geometrical properties of the network such as average connectivity, cross-linking and branching distance.[4,8–15] One of the generic mechanical features of these structures is their nonlinear strain-stiffening behaviour. The nonlinear stiffening is ubiquitous in biological systems and is apparent in the rapid increase of the material stiffness when subject to strain.[8,16–22] This makes them compliant to small deformations and resistant to large deformations. An increased resistance to large strains can act as a protection mechanism against tissue damage.[12,21] The property of a strain dependent stiffness of biopolymers has also inspired recent efforts to create synthetic polymers with similar properties.[23]

Several experimental and theoretical studies have focused on understanding the nonlinear mechanics of filamentous networks.[8,21,24–33] This striking behaviour can be understood for both thermal (entropic) and athermal (enthalpic) models. Affine thermal models are based on the nonlinear force-extension relation for individual semiflexible filaments between network junctions,[34,35] where the entropic stretching of the filaments or cross-linker proteins leads to a reduction in the amplitude of the transverse thermal undulations that in turn gives rise to a dramatic entropic strain stiffening.[8,21,24] The origins of stiffening in athermal models in contrast lie in non-affine collective deformation of the fibrous networks composed of interconnected elastic rods,[27,36–41] which can result in a nonlinear mechanical response at the network level, even for networks composed of purely linear elastic elements.[24,27,29,42]

Many experiments have been performed on reconstituted networks of biopolymers.[4,8,11,13,17,21] These constitute a new class of biological soft matter systems with remarkable material properties. Moreover, studies on these yield valuable input and tests for theoretical modeling of extracellular matrices and the cytoskeleton *in vivo*.[9,22,24,31,32,43]

Although intracellular networks, extracellular matrices and whole tissues show many similar mechanical properties, there are several important differences. Extracellular matrices tend to be much more open structures with larger pore size, making them more compressible than the typically finer intracellular meshworks on the same time-scales: as the incompressible fluid flows in and out, the networks can effectively change their volume. Also, extracellular biopolymers tend to have a larger persistence length. This is in particular true of collagen, which forms networks that can be treated as athermal and fully mechanical.[22,31,32,44,45]

[a] Department of Physics and Astronomy, VU University, Amsterdam, The Netherlands. E-mail: fcm@nat.vu.nl
[b] Institute for Medicine and Engineering, University of Pennsylvania, Philadelphia, PA, USA

In several studies, the mechanical response of tissues under compression/extension has been investigated.[16,46–53] It has been found that tissues exhibit stiffening under compression.[16,46,51–53] In addition, some reports have also reported some stiffening under extension.[16,46,50] Incompressible continuum models and finite element methods have been exploited to describe such behaviour.[46,54–56]

In contrast, biopolymer networks, including collagen matrices similar to the networks in whole tissues soften under compression and stiffen under extension[45] on time scales long enough for influx/efflux of interstitial fluid. As we discuss here, one difference between the two systems, tissues and extracellular networks, is closely related to the difference in the applied boundary condition. This behaviour is also completely different from that of the linear synthetic polymers such as polyacrylamide that do not show any stiffening for the same range of uniaxial strains.[45] Here, we consider disordered lattice-based network models with comparable average connectivities (coordination number) to real biopolymer networks.[57] The networks consist of bendable and stretchable fibres. By applying a fixed (lateral) boundary condition on our network under uniaxial strain, we can account for the mechanical behaviour we observe for reconstituted fibrin and collagen hydrogels. We also show that applying a global volume constraint on the network results in stiffening for both compression and extension.

Here, we focus on the effect of prestress, in the form of network extension and compression, on the properties of these networks. These are important aspects that have not received as much attention as shear rheology in recent work.[45] Prestress, in which residual stresses exist in an unloaded sample, happens frequently in cells and tissues.[58,59] Prestress can be natural and useful, *e.g.*, in the cardiovascular system, where it can increase pressure resistance,[60] and in cells, where myosin II motors can increase cell/gel stiffness by the generation of active, internal stresses.[61–63] Moreover, in blood clots, active, contractile stresses due to platelets are vital for wound closure.[64] But, prestress alteration can also be harmful as in pathologic conditions including hypertension and atherosclerosis.[65,66] Generally, the mechanical properties of prestressed systems differ from relaxed systems, due to intrinsic nonlinearities. Experiments have shown that biopolymer networks polymerized in the rheometer develop normal stresses.[45] Though the origins of such normal stress are not always understood, it is evident that the mechanical response of the network is influenced by such initial stresses.[31] It has also been shown that active agents such as molecular motors acting on networks can give rise to increased stiffness[63,67] and normal stress.[68] However, even in the absence of active agents, normal stresses can arise as in the polymerization process or simply due to an initial extension or compression applied to the network prior to subjecting the network to a shear deformation. The latter is the approach followed by ref. 45. Here, we systematically investigate the nonlinear mechanics of networks that have been subjected to an initial uniaxial deformation. We focus primarily on a computational model that can account for experiments in ref. 45, as well as new experiments presented here. We show that the prestress due to the initial deformation impacts the linear shear modulus and the onset of stiffening in the nonlinear shear stiffening curves.

The paper is organised as follows: Section 2 briefly describes the network model used here. Section 3 concisely explains the experimental methodology. In Section 4, we show the effects of prestress in the form of extension and compression on linear shear modulus and the nonlinear strain-stiffening both in experiments and simulation. We conclude in Section 5 with a brief summary and present our conclusions.

2 Model

To study the mechanical properties of biopolymer networks, we employ a minimal model to generate disordered, lattice-based networks. The networks are based on 2D triangular or 3D face-centred cubic (FCC) lattices with lattice spacing, l_0. Starting from these networks, we use a phantomization process to generate phantom networks with a local coordination number or connectivity $z = 4$, since higher connectivities are unphysical in experimental systems for networks consisting of cross-linked fibres ($z = 4$) and branching ($z = 3$). This phantomization is done for 2D networks by modifying triangular lattices such that at every lattice vertex, where three fibres cross, one filament is chosen at random and disconnected from the other two, allowing it to move freely as a phantom chain with no direct mechanical interaction with other two filaments.[69] For the 3D FCC lattice, where six fibres cross at each node, we randomly choose three independent pairs of cross-linked filaments.[70] The phantomization procedure, sets the connectivity of the respective networks precisely to $z = 4$. We further dilute the networks by random removal of bonds (fibre segments) between vertices. This is done to achieve the desired connectivity z, where $3 < z < 4$. It is also possible to reach this connectivity by only using the dilution process. The resulting networks are then called 2D diluted triangular lattices. We also ensure that there are no fibres spanning the full network.[70]

Importantly, this procedure results in a disordered network structure, in spite of the initial, regular lattice structure. Moreover, the resulting connectivity lies below the threshold of marginal stability for purely pairwise central-force interactions in both 2D and 3D, as identified by Maxwell:[71,72] this threshold is twice the dimensionality of the system. This means if spring-like interactions were the only relevant contribution to the Hamiltonian, these structures should be floppy and unstable. Networks of biopolymers are, however, stable 3D structures with average connectivity below this isostatic threshold.[57] In fact, such sub-isostatic networks can be rigid due to additional stabilising interactions, such as bending,[10,36,37] internal or applied stresses[31,73,74] or thermal fluctuations.[75] Here, we include bending interactions in our model. To reduce any edge effects, periodic boundaries are imposed with Lees–Edwards boundary conditions.[76] The cross-links or branching points are permanent in our networks and they hinge freely with no resistance. Prior simulations of networks consisting of cross-linked or branched fibres,[10,77,78] with and without freely-hinged cross-links, have shown very

similar behaviour in mechanical properties for the same average connectivity z. This suggests that additional bending interactions at the cross-links, as can be expected for both fibrin and collagen, will not significantly affect our model predictions.

The filaments in the network are described by an extensible wormlike chain (EWLC) model (bending and stretching contributions) and the Hamiltonian of the system $\mathscr{H}$ is obtained by summing over all the fibres,[36] f:

$$\mathscr{H} = \sum_f \left[\int \frac{\kappa}{2} \left| \frac{\mathrm{d}\hat{t}}{\mathrm{d}s_f} \right|^2 \mathrm{d}s_f + \int \frac{\mu}{2} \left(\frac{\mathrm{d}l}{\mathrm{d}s_f} \right)^2 \mathrm{d}s_f \right]. \quad (1)$$

Here, κ is the bending rigidity of the individual filaments, μ is their stretch modulus and, $\hat{t}$ and $\mathrm{d}l/\mathrm{d}s_f$ are the unit tangent and longitudinal strain respectively at a point s_f along the fibre contour. Here, we only consider athermal networks, which have been shown to successfully capture the mechanics of collagen networks.[31,32] Although the individual elements of the model are linear, the network mechanics are highly nonlinear. The schematic of the model in 2D is shown in Fig. 1.

The dimensionless bending rigidity is defined as $\tilde{\kappa} = \kappa/(\mu l_0^2)$ which we vary in our networks while keeping $\mu = 1$ constant. For 3D networks based on FCC lattices, l_0 is the same as the distance between the cross-links, l_c. For 2D phantom networks, the average distance between the cross-links is somewhat larger,[79] $l_c \simeq 1.4 l_0$ for $z \simeq 3.3$. Given a homogeneous cylindrical rod of radius r and Young's modulus E, from classical beam theory,[80] $\mu = \pi r^2 E$ and $\kappa = \frac{\pi}{4} r^4 E$. From this, $\tilde{\kappa} = \frac{1}{4} r^2/l_0^2$, which is proportional to the protein volume fraction ϕ, which can be seen as follows. Within a volume l_0^3 in the network, there will be of order one fibre segment of volume, $\pi r^2 l_0$, corresponding to a volume fraction[45] $\phi \sim r^2/l_0^2 \sim \tilde{\kappa}$. Hence, the most relevant values of $\tilde{\kappa}$ for biopolymer systems range from[31,69] 10^{-4} to 10^{-2}.

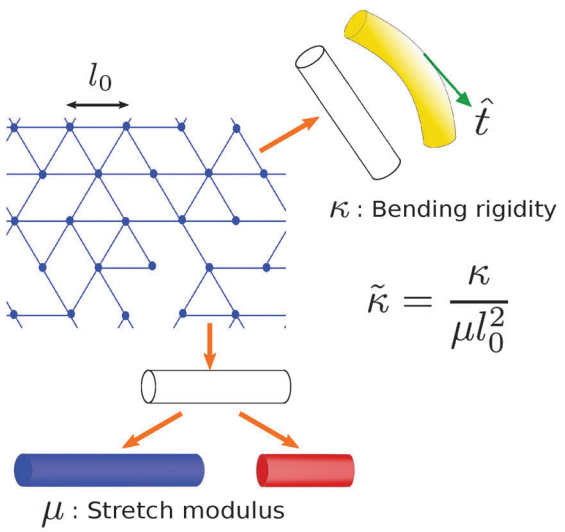

Fig. 1 2D schematic representation of the model: the network is a 2D diluted triangular lattice with lattice spacing, l_0. Each bond is assumed to act like a spring with stretch modulus, μ. The blue and red colouring of the filament shows its extension and compression. Fibres can also bend at the hinges with bending rigidity, κ which is shown by the yellow bent fibre. The dimensionless parameter, fibre rigidity, $\tilde{\kappa}$ is then defined as the ratio between the bending rigidity, κ and stretch modulus, μ where l_0^2 is used for dimensional purposes, $\tilde{\kappa} = \kappa/(\mu l_0^2)$.

Although $\tilde{\kappa}$ is naturally related to the volume fraction of the gel, it is not independent of the type of biopolymer. For instance, given expected differences in the Young's modulus and fibre diameter between collagen and fibrin, one cannot necessarily directly compare, *e.g.*, the ratio of collagen to fibrin concentrations with a ratio of $\tilde{\kappa}$ values. One can, for a single polymer type, compare a ratio of concentrations with a corresponding ratio of $\tilde{\kappa}$ values, as shown in both ref. 31 and 32. We have used these prior references to help us choose appropriate parameters for collagen. For fibrin, however, we do not have an independent way of determining $\tilde{\kappa}$. Thus, this parameter should be considered to be an undetermined fit parameter.

To find the elastic stresses or responses of these networks, the relevant deformation is applied to the network and then the energy is minimised using the conjugate gradient minimisation method.[81] We are in particular interested in shear stress, σ_s, the storage modulus, G, and normal stress, σ_N, all of which are obtained using the minimised total elastic energy, E. Shear stress is calculated from the derivative of the minimised elastic energy density E/V of the network, where V is the system area (volume) in 2D (3D), with respect to the applied shear strain, γ:

$$\sigma_s = \frac{1}{V} \frac{\partial E}{\partial \gamma}. \quad (2)$$

From this, the storage modulus is obtained as the ratio

$$G = \frac{\sigma_s}{\gamma}. \quad (3)$$

The normal stress, σ_N, is calculated from the derivative of the energy with respect to uniaxial strain ε:

$$\sigma_N = \frac{1}{V} \frac{\partial E}{\partial \varepsilon}. \quad (4)$$

Our simulation results are in units of μl_0^{1-d}, where d is the dimension of the system. All the simulation results are carried out on large enough systems sizes to minimise finite size effects. In an undiluted network, we use in 3D, 30^3 nodes and 50^2 nodes in 2D for all the reported results unless otherwise specified. The probability of existing bonds in 3D networks is $p = 0.85$, in 2D phantom networks is $p = 0.9$ and in 2D diluted triangular networks is $p = 0.58$.

In the simulation, both 2D and 3D networks are studied, although biopolymer networks are inherently 3D structures. Recent computational studies of the lattice-based networks have shown remarkable quantitative agreement between 2D and 3D networks, both in their linear and nonlinear mechanical behaviour, provided that the networks have the same connectivity z and are below the 2D isostatic threshold.[32,79] The elasticity of 2D networks can be mapped to those from 3D by correctly accounting for the line density[79] $\rho \propto l_0^{1-d}$. Moreover, the overall elastic properties of lattice- and off lattice-based network models have been demonstrated to be similar.[31,32,79]

For comparison with experiments, we use fixed lateral boundaries, for which the ratio of normal stress to uniaxial strain gives the longitudinal modulus $M = \sigma_N/\varepsilon$ for small strains ε. These boundary conditions are most relevant to extracellular networks of collagen and fibrin in a rheometer, for which the lateral dimension is typically much larger than the axial dimension (*i.e.*, gap size). For networks that adhere to the axial boundaries (rheometer plates), this aspect ratio, together with the open network structure and flow of fluid in and out during rheological measurements, leads to effectively fixed lateral boundaries and a vanishing of the (apparent) Poisson ratio.[45] Here, we investigate the effect of uniaxial deformation on the shear and normal stresses and storage modulus of the networks. To apply uniaxial deformation to our networks, the length of the system in the direction perpendicular to the shear stress is initially rescaled. For example, to have a system subject to 10% compression (extension), the axial length of the system is decreased (increased) accordingly. After applying this global deformation, the energy of the network is minimised before applying any shear measurements. This is similar to having a system in the prestressed state before these measurements. Then the effect of this prestress on the linear shear modulus and nonlinear shear strain-stiffening curves are investigated. It is important to note that fibrin is known to differ from collagen at high strain/stress. Fibrin fibers undergo significant and nonlinear stretching, for which protein unfolding has recently been implicated.[82–85]

3 Experimental

To prepare collagen networks, collagen type 1 (isolated from calf skin, MP Biomedicals, Santa Ana, CA, USA), 10× phosphate-buffered saline (PBS), 0.1 M NaOH and ddH_2O were warmed to room temperature and added in appropriate ratios to yield a 2.5 mg ml^{-1} collagen concentration in 1× PBS solution with a neutral pH. To prepare fibrin networks, fibrinogen (Fbg) stock solution (isolated from human plasma and plasminogen depleted, CalBioChem, EMD Millipore, Billerica, MA, USA,) 1× T7 buffer (50 mM Tris, 150 mM NaCl at pH 7.4), $CaCl_2$ stock and thrombin (isolated from salmon plasma SeaRun Holdings, Freeport, ME, USA) were added at appropriate ratios to yield 2.5 or 10 mg ml^{-1} fibrinogen, 30 mM Ca^{2+} and 0.5 U thrombin per mg of Fbg. Samples are polymerized between the parallel plates of a rheometer or tensile tester. Samples are completely surrounded by the buffer thus the fluid can flow in and out freely.

The rheology data were acquired similarly as in ref. 45 Briefly, a strain-controlled rheometer (RFS3, TA Instruments, New castle, DE, USA) was used in a parallel-plate configuration with plate diameters of 8 mm, 25 mm or 50 mm. Uniaxial strain was applied by changing the gap between the plates after sample polymerization, shear strain was applied by rotating the bottom plate. The upper plate was connected to a force sensor measuring both torque and normal force. Shear moduli were calculated by accompanying rheometer software (TA Orchestrator). Normal stress was calculated by dividing the force measurements by the plate area. Uniaxial strain dependence was tested by recording the shear moduli and normal force in time, at a constant frequency of 10 rad s^{-1} and low shear strain of 2%, while applying step-wise uniaxial strain and letting the samples relax in between steps for 100–1200 seconds, depending on the sample and step size. The normal stress measurements were complemented with tensile tester measurements (Instron 5564) using the same testing set-up as with the shear rheometer. Shear strain amplitude dependence was tested by applying shear strain at a constant frequency of 1 rad s^{-1}, while increasing the shear strain amplitude logarithmically with 20 pts per decade starting at 2% shear strain.

4 Results and discussion: elastic properties of networks under extension and compression

Under typical physiological conditions, tissues in the body are constantly subjected to complex deformations. It is thus important to see how the mechanical properties of such systems vary under application of both shear as well as axial strain. As mentioned in the introduction, reconstituted networks of biopolymers are good candidates for studying real biopolymer scaffolds. In this work, we investigate the role of prestress generated by the uniaxial strain on the mechanical properties of extracellular networks of collagen and fibrin.

We compare experimental results with simulation results from 2D and 3D networks (see Model section). In order to compare the results from simulation to our experiments, we apply fixed lateral boundary conditions. Our 2D and 3D networks have comparable average connectivities as those observed in the extracellular networks.[57] Both experimental and computational results show softening for compression and stiffening for extension (which is different from the results obtained from the measurements on tissue).[16,46,50–53] We focus on the impact of prestress generated due to the uniaxial strain on the mechanical properties of these systems. In subsection 4.1 the impact on the linear shear modulus and in 4.2 the strain-stiffening curves are considered. In both subsections (4.1 and 4.2), the effect of uniaxial strain on normal stresses is also investigated. In subsection 4.3, we discuss the effect of global volume boundary condition on the simulation results which imposes the incompressibility condition on the networks.

4.1 Effect of prestress on linear shear modulus

We investigate the role of uniaxial strain in the form of extension or compression on the linear shear modulus. Experimentally, the samples are subjected to an incremental series of compression/extension. At any given uniaxial deformation, the dynamic shear modulus is measured at an amplitude of 2% shear strain and frequency of 10 rad s^{-1}. In between each compression/extension step, the networks are allowed to relax for 100 to 1200 seconds depending on the step size or sample. A tensile tester is used to

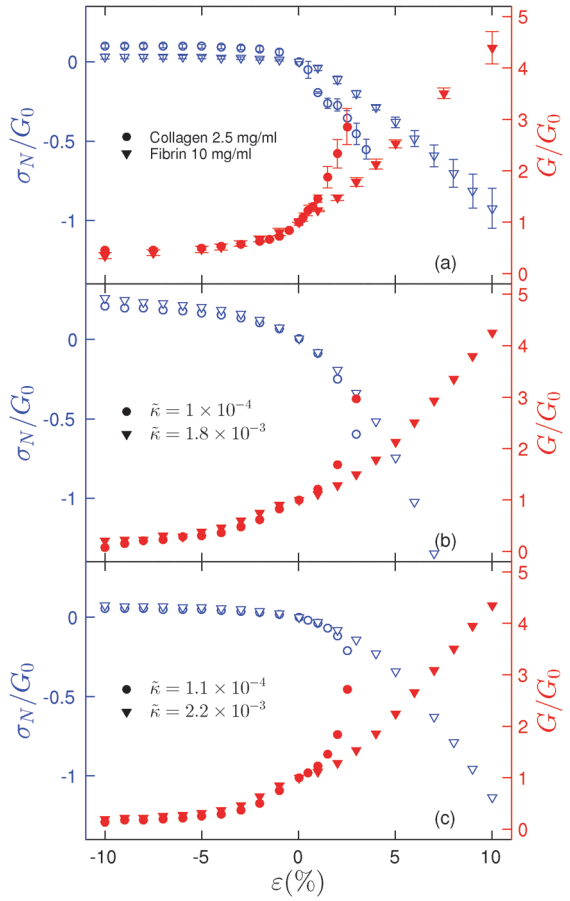

Fig. 2 Normal stress (σ_N) (unfilled blue symbols) and linear shear modulus (G) (filled red symbols) *vs.* uniaxial strain (ε): (a) data from measurements on collagen (2.5 mg ml^{-1}) (○) and fibrin (10 mg ml^{-1}) (▽).[45] The range of linear shear elasticity is approximately 5–10% in both cases.[45] The normal stress is set to zero before doing the measurements. (b) Data from simulations on a 3D phantom lattice for two different $\tilde{\kappa}$ values, 1×10^{-4} (○) and 1.8×10^{-3} (▽). (c) Data from simulations on a 2D phantom lattice for two different $\tilde{\kappa}$ values, 1.1×10^{-4} (○) and 2.2×10^{-3} (▽). The data in the three panels are normalised by the linear shear modulus of the unloaded network ($\varepsilon = 0$), G_0. In the simulations, network with lower fibre rigidity which resembles behaviour of collagen, stiffens faster. There is a good qualitative agreement between theory and experiment.

measure the uniaxial stress of the samples after relaxation for similar levels of uniaxial strain.

Similarly, in the simulations, the networks are subjected to successive 1% increments of either compression or extension. After each step, the energy is first minimised and the normal stress σ_N is calculated before measuring the linear shear modulus. To measure this, small shear strain (1%) is applied and again the energy of the network is minimised before applying the next uniaxial strain step. This process continues over the full ±10% uniaxial strain range, with fixed lateral boundary conditions. The results are shown in Fig. 2. We use the following sign convention: positive uniaxial strains represent extension, while negative values indicate compression. As expected, when the networks are compressed, both experiments and simulations show positive normal stresses, corresponding to compressive stresses that would lead to expansion in the absence of applied external stress. In Fig. 2a, normalised shear modulus G and normal stress σ_N are shown *versus* uniaxial strain ε for both 2.5 mg ml^{-1} collagen and 10 mg ml^{-1} fibrin networks. As can be seen here, the linear shear modulus changes under uniaxial strain. Both fibrin and collagen samples stiffen under extension but soften under compression.[45] Moreover, the collagen samples stiffen more rapidly under extension than do the fibrin samples.

In the experiments, the normal stress is always set to zero before doing the measurements. This can be seen from the data where we have zero normal stress at $\varepsilon = 0$ in Fig. 2a. In Fig. 2b, G and σ_N for two phantomized 3D FCC networks with fibre rigidities $\tilde{\kappa} = 1 \times 10^{-4}$ and $\tilde{\kappa} = 1.8 \times 10^{-3}$ are shown. In Fig. 2c, G and σ_N for two 2D phantom networks with $\tilde{\kappa} = 1.1 \times 10^{-4}$ and $\tilde{\kappa} = 2.2 \times 10^{-3}$ are plotted. As noted above, $\tilde{\kappa}$ is expected to be proportional to the volume fraction. Thus, the larger value implied for fibrin is qualitatively consistent with the higher fibrin concentration. In Fig. 2, the linear shear modulus of unloaded networks is used to normalize the curves. These results are very different from those of tissues.[16,46,50–53] As can be seen in Fig. 2, both 2D and 3D networks agree qualitatively well with the experimental results. Considering also prior experimental results in ref. 45, the qualitative behaviour of the elastic properties *versus* uniaxial strain appears to be rather insensitive to concentration in experiments and to $\tilde{\kappa}$ in simulations.

The similarity of our results for 2D and 3D networks is consistent with prior simulations. In ref. 79, for instance, very good quantitative agreement was shown between 2D and 3D network shear response, both linear and even highly nonlinear, provided that one compares networks with the same average connectivity $\langle z \rangle$, and one accounts for the effectively different concentrations of fiber (measured as line length per unit area/volume in 2D/3D). The strain thresholds were even shown to be in quantitative agreement between 2D and 3D for networks with the same average connectivity $\langle z \rangle$, so long as this is well below the corresponding isostatic (Maxwell) thresholds in the respective dimensions. Realistic networks of both collagen and fibrin satisfy this latter condition for both 2D and 3D. In what follows, we show primarily simulation results from 2D networks. We have done this mostly in order to reduce finite-size effects, since we are able to achieve larger linear dimensions in 2D networks.

In Fig. 2, we note that for positive uniaxial strain $\varepsilon > 0$, the magnitude of the normal stress shows similar behaviour to the shear modulus: in both the model and experiment, as the shear modulus G increases under extension, so does $|\sigma_N|$, although σ_N is negative under (positive) uniaxial strain. In fact, under extension ($\varepsilon > 0$), the change in the shear modulus $G - G_0$ relative to the unstrained value G_0 at $\varepsilon = 0$ is predicted to vary approximately linearly with σ_N, as shown in Fig. 3a. The predicted dependence of $G - G_0$ on σ_N is consistent with fibrin at 2.5 and 10 mg ml^{-1} indicated in Fig. 3b. In Fig. 3, for simulations and experiments, both axes are normalised by the corresponding shear modulus, G_0. The resulting dimensionless data allow for a direct quantitative comparison of simulation

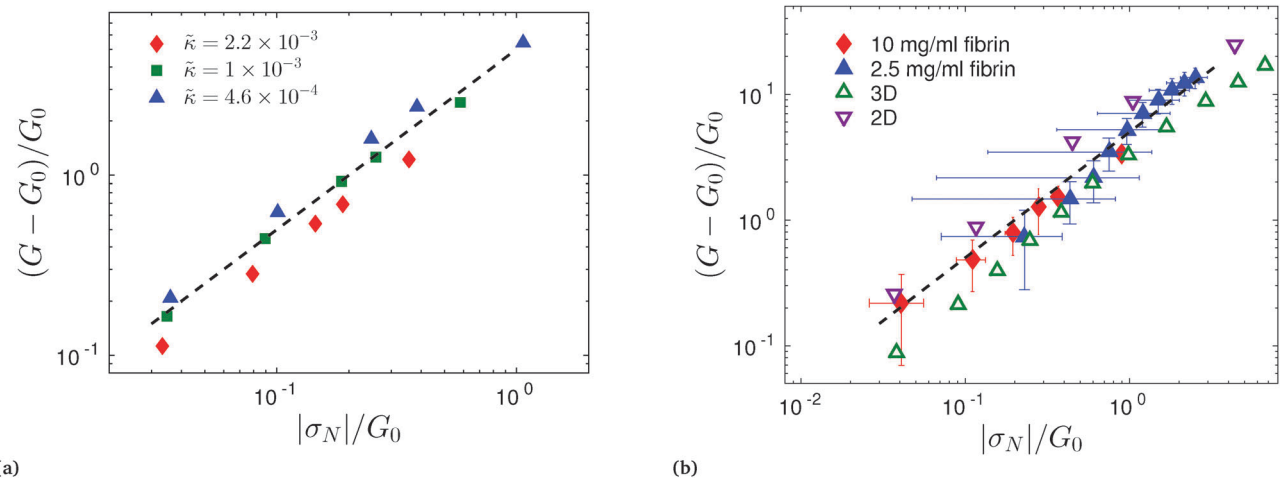

Fig. 3 The normalised increase in linear shear modulus after extension *versus* the corresponding change in magnitude of normal stress: (a) data from simulations on 2D diluted phantom triangular lattice with different $\tilde{\kappa}$. The normalisation is with respect to G_0. The dashed line with slope one represents $(G - G_0) = 5|\sigma_N|$, corresponding to a good approximation for $\tilde{\kappa} = 10^{-3}$. This same line is superimposed in (b) showing excellent quantitative agreement with experiments in that panel. In (b), data (filled symbols) are shown for fibrin samples at 2.5 mg ml^{-1} and 10 mg ml^{-1}. These have also been normalised by G_0. Moreover, the unfilled upright (green) triangle data shows 3D simulation results for a network with $\tilde{\kappa} = 10^{-4}$ and the unfilled inverted (purple) triangle data are 2D simulation results for a network with the same bending rigidity as that of 3D network.

with experiment. The dashed line in both panels of Fig. 3 corresponds to $(G - G_0) \simeq 5|\sigma_N|$ for $\tilde{\kappa} = 10^{-3}$, which agrees to within a factor of two with both 2D and 3D simulations for $\tilde{\kappa} = 10^{-4}$, as well as experiments. Prior work on collagen[31] and model networks with compliant crosslinks[86] have also reported an approximate linear scaling of modulus with the normal stress. Interestingly, we also observe in Fig. 3 an apparent systematic difference of approximately a factor of three between 2D and 3D. This may be due to the effectively stronger influence of lateral boundaries in 3D compared with 2D: in 3D, the fixed boundaries occur along two lateral axes, while there is only a single lateral axis in 2D. With this in mind, it may not be surprising that the experiments appear to be intermediate between 2D and 3D, since some radial relaxation of the sample is possible experimentally, which is not accounted for in the simulations.

4.2 Strain-stiffening and its dependence on prestress

We now consider the following questions: (1) how do the shear strain stiffening curves change with applied extension and compression? (2) How does the onset of shear strain stiffening change for different prestressed states? (3) How does the normal stress vary when we apply nonlinear shear deformation to prestressed networks? The samples are first subjected to an applied static compression/extension in a strain-controlled rheometer with parallel plates. The uniaxial strain is applied by changing the gap size between the two plates. As in our previous measurements, volume change is allowed by surrounding the sample with solvent. An oscillatory shear strain of constant frequency of 1 rad s^{-1} with an increasing magnitude is subsequently applied. The shear storage modulus is then measured. In the simulations, 2D and 3D diluted phantom networks are first compressed/extended with similar amounts of uniaxial strains as in the experiments, after which the energy of the network is minimised. Normal stresses are calculated and then by keeping the uniaxial strain fixed, the network is subjected to increasing shear deformation from 1% until 100% in logarithmic steps. After each shear step, the energy of the system is again minimised and the storage modulus is calculated.

In Fig. 4a, the strain-stiffening curves from a 2D diluted phantom lattice with fibre rigidity $\tilde{\kappa} = 2.2 \times 10^{-4}$ are shown for different amounts of uniaxial strains. In Fig. 4b, the nonlinear strain-stiffening curves from 2.5 mg ml^{-1} fibrin samples are presented for different amounts of prestress. The stiffening curve for 0% uniaxial strain is also shown in both panels for comparison. Both simulation and experimental results are normalised by the linear shear modulus G_0 of the unloaded network. As can be seen in Fig. 4, the experimental results show good qualitative agreement with the simulation results. Extended networks are stiffer and compressed networks are softer. The variation in the onset of stiffening for different uniaxial strains also shows similar behaviour as in the simulation results. By applying compression the onset of stiffening shifts towards larger strains relative to the case without any uniaxial load suggesting that nonlinear behaviour is delayed. The more compressed the sample, the larger the shear strains at which the nonlinear behaviour is seen. This can be understood within a simple physical picture, in which network compression results in fibres that buckle or bend due to the smaller energy cost for bending than compression (see Fig. 5a and b). This, in turn, results in a reduced end-to-end distance of the fibres and an excess length[31,79] (the difference between contour length and end-to-end distance). This excess length delays the shear strain onset of fibre stretching. Thus, compression shifts the onset of stiffening to larger shear strains. In contrast, the inverse happens for extended networks. The smaller excess length results in smaller onset of stiffening. The shift in the

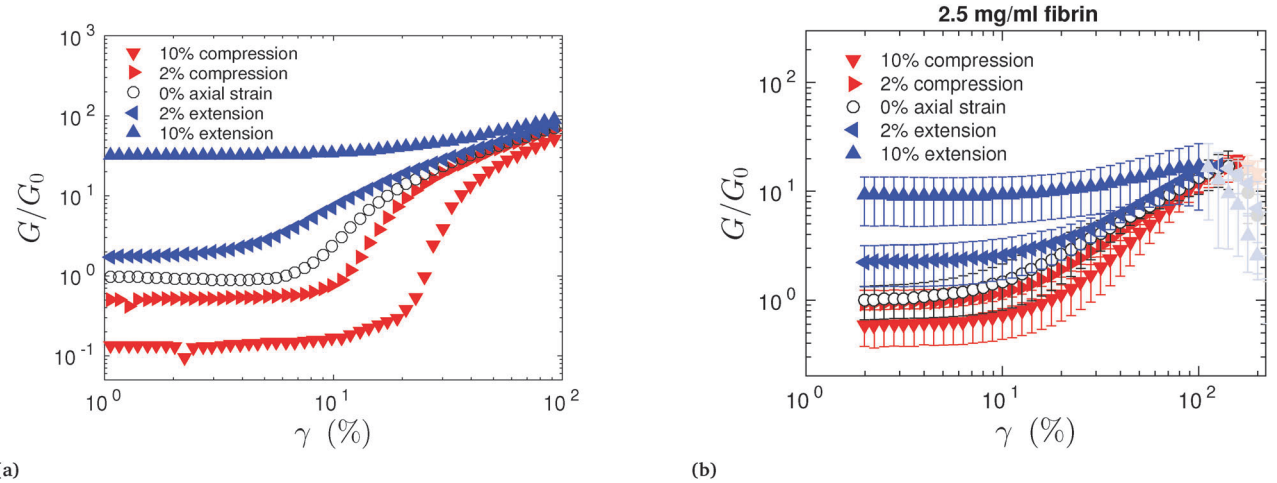

Fig. 4 Normalised storage modulus G *vs.* shear strain γ for networks with imposed uniaxial strains. The results for the unloaded networks are shown for better comparison. Linear shear modulus G_0 of the unloaded sample is used for normalisation: (a) data from simulations on 2D phantom networks with $\tilde{\kappa} = 2.2 \times 10^{-4}$. (b) Data from measurements on fibrin (2.5 mg ml^{-1}). The error bars are also shown. The downturn in the curves for strains larger than ~100% corresponds to sample detachment from the plates. The corresponding data are shown with lighter colors. Strain-stiffening curves are qualitatively similar for the loaded networks both in experiments and simulation to the unloaded network. The only case which shows a significant deviation is the most extended network ε = 10% where strain-stiffening is less pronounced. Compressed networks start from lower values thus they are softer. Extended networks lie above the unloaded network and so they are stiffer. The onset of stiffening shifts to the right (higher strains) for the compressed networks and it shifts to lower strains for extended networks with the exception of the most extended sample ε = 10%.

onset to lower strains with the applied extension occurs only over a limited range of uniaxial extension. Beyond a certain extension, it appears that the strain threshold for the onset of stiffening increases with the applied extension. This happens because beyond a certain extension, no excess lengths can build up in the fibres. In fact, after a sufficiently large extension, the shear response of a network can be captured by the affine prediction. In an affinely deformed network, the elastic response is only governed by stretching modes for any applied shear strain.

It is informative to look into the variation of the normal stresses during shear stiffening and compare the results under varying amounts of prestress. Different studies investigated the normal stresses of biopolymer networks when sheared. The normal stresses of these networks are negative under shear[26,87] which are opposite in sign (direction) compared to those measured from most elastic solids. This is known as the Poynting effect.[88,89] From symmetry arguments, the normal stresses (if analytical) should only be functions of even powers of γ. For low strains, $\sigma_N \sim \gamma^2$ is expected based on symmetry considerations.[26,27,39,87] The absolute values of normal stresses of the same networks as in Fig. 4 and 5 are shown in Fig. 6. Again, for comparison, the results of the network with no uniaxial load is also shown. As expected, the normal stresses from simulation results for networks without uniaxial load initially show the γ^2 regime (see Fig. 6a). Extension and compression loads introduce opposite effects on the uniaxial response of the network. When networks are extended, they tend to pull the boundary downward (negative normal stress) while compression induces an upward (positive normal stress) response. The normal stress of the compressed networks start from positive values while the extended ones show negative values for low shear deformations. With increasing shear strain, the extended

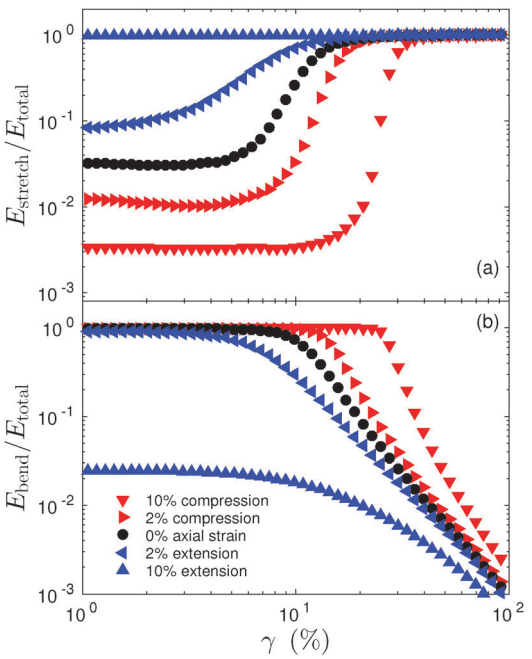

Fig. 5 Relative energy contributions for a 2D phantom network with $\tilde{\kappa} = 2.2 \times 10^{-4}$ and different applied uniaxial strain (ε) *vs.* shear strain, γ (a) relative contribution of total stretching energy to the total elastic energy of the network (b) relative contribution of total bending energy to the total elastic energy of the network. By applying extensive loads, the stretching energy contribution of the network gets larger and consequently the bending energy contribution gets smaller. In the case of 10% applied uniaxial extension, the network energy becomes initially dominated by stretching and one no longer sees a transition from bend-dominated to stretch-dominated behavior. Indeed, its response is increasingly becoming affine. The symbols in panel (a) are the same as in panel (b).

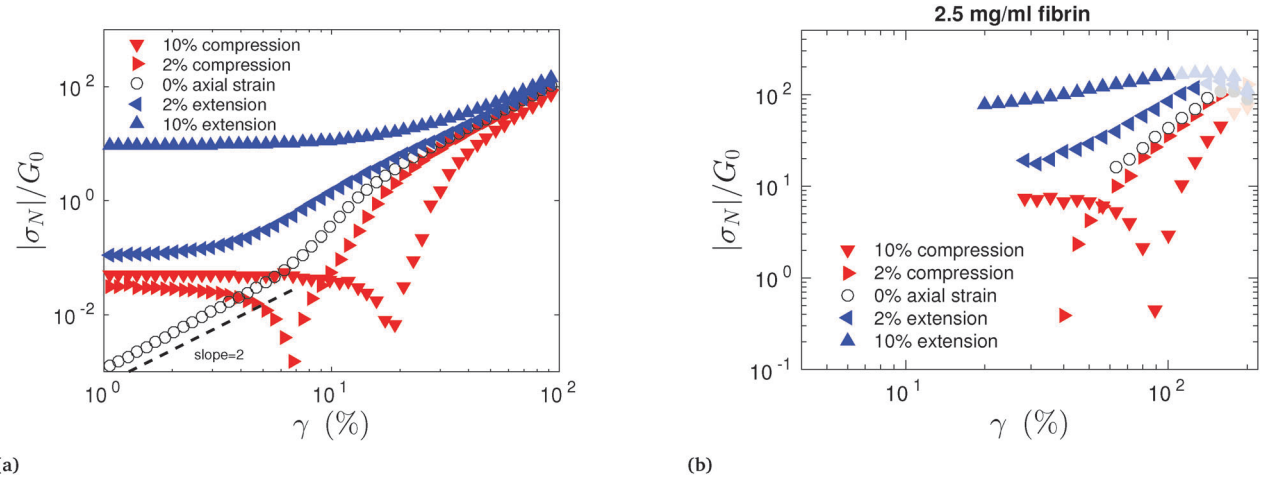

Fig. 6 Absolute value of the normal stress ($|\sigma_N|$) *vs.* shear strain γ for different applied uniaxial strain (a) data from simulations on a 2D phantom network with $\tilde{\kappa} = 2.2 \times 10^{-4}$. We can see that the normal stresses in the cases with imposed uniaxial compression and extension do not show the expected γ^2 dependence in the no uniaxial case. (b) Data from measurements on fibrin (2.5 mg ml^{-1}). The data corresponding to the downturn in storage modulus curves (see Fig. 4b) are shown with lighter colors. In both theory and experiment, the normal stresses in the extended networks are always negative but the normal stresses in the compressed networks change sign from the initial positive to negative values. The dip in the compressed networks show the sign change of the normal stress. The normal stress values are normalised by the linear shear modulus G_0 of the network with no imposed uniaxial strain.

networks show even larger negative normal stresses while the initial positive normal stresses of the compressed networks decrease in magnitude, then cross over at zero to switch sign. The dip in the normal stress of the compressed networks (in absolute value) show the sign change. It might seem that the strain at which the sign change of the normal stress occurs coincides with the onset of stiffening. However we find that it is not the case. The experimental results shown in Fig. 6b are similar to those of the model, although the strain threshold for the sign change for the normal stress is higher by a factor of approximately five in experiments. Experimentally, the smaller normal stresses corresponding to lower strains are somewhat difficult to resolve due to device limitations. The data corresponding to the downturn in storage modulus curves of Fig. 4b are shown with lighter colors.

It has been demonstrated that for the network without an imposed uniaxial strain, shear and normal stresses become comparable at the onset.[31,87] In Fig. 7, we show shear stress, storage modulus and normal stress *versus* shear strain. We consider the three cases: no uniaxial strain, compression and extension. The linear shear modulus G_0 has been used for the normalisation. Normal and shear stresses become comparable at the onset of stiffening. This holds for unloaded and compressed networks (see Fig. 7a and b). However, for extended networks, this is not the case (see Fig. 7c). Here, at the onset of stiffening, the shear stress is still smaller than the normal stress. It is important to note that the onset of stiffening does not coincide with the shear strain at which normal stress changes sign as seen in Fig. 7b.

4.3 Tissues and global volume constraint boundary condition

As seen in the previous subsections, experimental and computational results show softening for compression and stiffening for extension of biopolymer networks in solvent, which is in

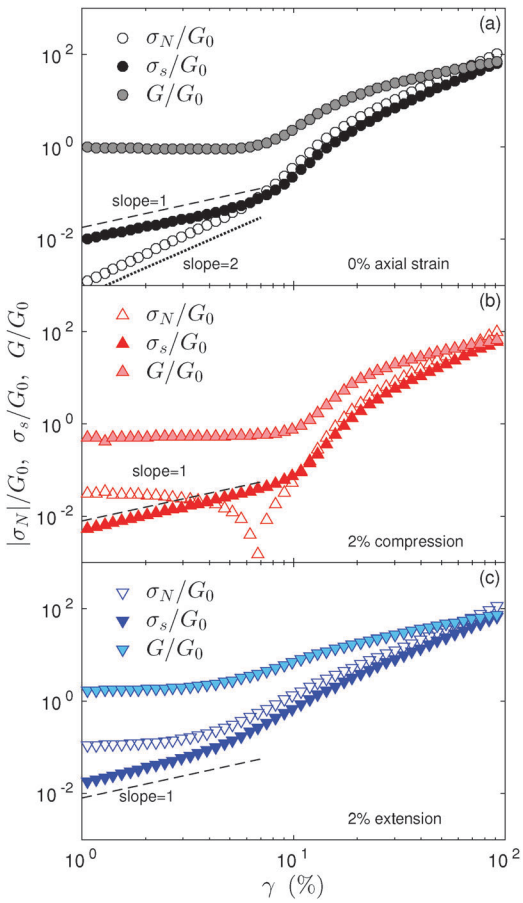

Fig. 7 Comparison of the normalised shear σ_s and normal stresses σ_N and storage modulus G *versus* shear strain γ. Linear shear modulus G_0 of the unloaded network has been used for all the normalisations. At the onset of stiffening, normal and shear stresses become comparable for unloaded networks which has been noticed both theoretically and experimentally (panel a).[31,87] This is still the case for compressed networks (panel (b)). For extended networks, this is not the case (panel (c)).

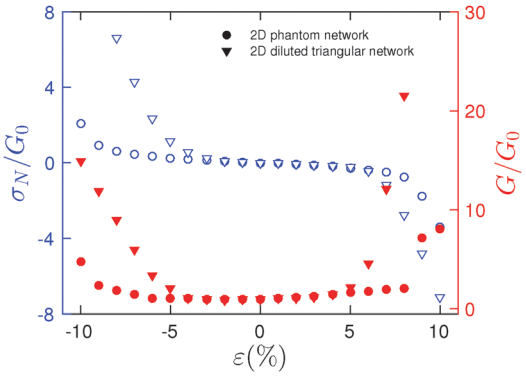

Fig. 8 Normalised normal stress (unfilled blue symbols) and shear modulus (filled red symbols) for 2D phantom triangular ($\langle z\rangle$ = 3.2) and 2D diluted triangular networks ($\langle z\rangle$ = 3.3) both with fibre rigidity, $\tilde{\kappa} = 10^{-4}$ under uniaxial extension and compression with global volume constraint boundary condition. The data are normalised by the shear modulus at zero uniaxial strain G_0. We see stiffening for both compression and extension. Here we use networks of 30^2 nodes.

contrast with experimental reports of stiffening under compression for tissues.[51–53] This property can be seen in our networks if we apply appropriate boundary conditions for incompressibility, in which the sample expands (contracts) laterally under uniaxial compression (expansion). For incompressible 2D networks, the lateral strain is equal and opposite to the axial strain, corresponding to a Poisson ratio of unity.

In Fig. 8, we have used the 2D network model similar to the previous subsections with the only difference being the global volume constraint, to impose the incompressibility condition. The difference between the two curves is their corresponding network structure. We show the result for a 2D phantom network with $\langle z\rangle$ = 3.2 and a 2D diluted triangular network with $\langle z\rangle$ = 3.3 for which this connectivity is reached by random bond removal. We observe stiffening for both uniaxial compression and extension. The strain at which stiffening starts (about 5% for 2D phantom network and about 8% for 2D diluted triangular network) or the shape (steepness) of the curve is dependent on the network structure as well as fibre rigidity. In 3D networks, considering the global volume constraint, the lateral strain is not the same as axial strain. Despite the Poisson ratio of one half in 3D, one would expect stiffening for both compression and extension.

5 Conclusions

We have studied the elastic properties of networks to which uniaxial strain has been applied. Specifically, we studied, both experimentally and in simulation, normal and shear stresses, as well as strain-stiffening and the linear shear modulus. The experimental results from reconstituted networks of fibrin and collagen have been compared with results from lattice-based networks with physiological connectivity, in both 2D and 3D. Networks in both 2D and 3D give similar behaviour for the same connectivity. In both cases, we find good qualitative agreement with experiments. In the experiments, the rheometer is surrounded with buffer allowing for water to freely move in or out. In simulations, fixed boundary conditions are used to be consistent with experiments. By using fixed boundary conditions, applied extension or compression results in a volume change. Prestress resulting from the applied extension and compression, strongly affects the network elastic response. Softening due to compression and stiffening due to extension are observed for both experiments and simulations. By applying a global volume constraint in order to account for the volume-preserving aspect of tissue,[16] our simulation results show stiffening for both extension and compression. The linear shear modulus increases with the normal stress and exhibits an approximately linear scaling with normal stress both in experiment and in simulation.

The strong dependence of the mechanics of extracellular networks on prestress can be expected to have important consequences for both fundamental tissue mechanics, as well as for tissue engineering. The softening of compressed samples and the dependence of the strain onset of stiffening, for instance, are likely to be important mechanical parameters for synthetic tissue scaffolds. Network simulations are powerful techniques to gain more insight into these mechanical parameters for the design of such scaffolds and other biocompatible materials.

Acknowledgements

M. V., A. S. and A. J. L. were supported by Stichting voor Fundamenteel Onderzoek der Materie which is part of the Nederlandse Organisatie voor Wetenschappelijk Onderzoek. A. S. was also partly supported by NanoNextNL. P. A. J., A. S. G. O. and P. A. G. were supported by grants NIH EB017753 and NSF-DMR-1120901. A. S. G. O. was supported by a Fulbright Science and Technology Award, and the Prins Bernhard Cultuurfonds-Kuitse Fonds. The simulations were done on the Dutch national e-infrastructure with the support of SURF Cooperative.

References

1 B. Alberts, A. Johnson, J. Lewis, M. Raff, K. Roberts and P. Walter, *Molecular Biology of the Cell*, Taylor & Francis Group, 2007.
2 A. R. Bausch and K. Kroy, *Nat. Phys.*, 2006, **2**, 231–238.
3 K. E. Kasza, A. C. Rowat, J. Liu, T. E. Angelini, C. P. Brangwynne, G. H. Koenderink and D. A. Weitz, *Curr. Opin. Cell Biol.*, 2007, **19**, 101–107.
4 O. Chaudhuri, S. H. Parekh and D. A. Fletcher, *Nature*, 2007, **445**, 295–298.
5 O. Lieleg, M. M. A. E. Claessens and A. R. Bausch, *Soft Matter*, 2010, **6**, 218–225.
6 D. A. Fletcher and R. D. Mullins, *Nature*, 2010, **463**, 485–492.
7 C. Frantz, K. M. Stewart and V. M. Weaver, *J. Cell Sci.*, 2010, **123**, 4195–4200.
8 M. L. Gardel, J. H. Shin, F. C. MacKintosh, L. Mahadevan, P. Matsudaira and D. A. Weitz, *Science*, 2004, **304**, 1301–1305.

9 R. Tharmann, M. M. A. E. Claessens and A. R. Bausch, *Phys. Rev. Lett.*, 2007, **98**, 088103.
10 C. P. Broedersz, X. Mao, T. C. Lubensky and F. C. MacKintosh, *Nat. Phys.*, 2011, **7**, 983–988.
11 M. L. Gardel, F. Nakamura, J. H. Hartwig, J. C. Crocker, T. P. Stossel and D. A. Weitz, *Proc. Natl. Acad. Sci. U. S. A.*, 2006, **103**, 1762–1767.
12 C. T. Koh and M. L. Oyen, *J. Mech. Behav. Biomed. Mater.*, 2012, **12**, 74–82.
13 B. Wagner, R. Tharmann, I. Haase, M. Fischer and A. R. Bausch, *Proc. Natl. Acad. Sci. U. S. A.*, 2006, **103**, 13974–13978.
14 H. Hatami-Marbini and R. C. Picu, *Acta Mech.*, 2009, **205**, 77–84.
15 K. A. Erk, K. J. Henderson and K. R. Shull, *Biomacromolecules*, 2010, **11**, 1358–1363.
16 Y. C. Fung, *Am. J. Physiol.*, 1967, **213**, 1532–1544.
17 P. A. Janmey, S. Hvidt, J. Käs, D. Lerche, A. Maggs, E. Sackmann, M. Schliwa and T. P. Stossel, *J. Biol. Chem.*, 1994, **269**, 32503–32513.
18 J. V. Shah and P. A. Janmey, *Rheol. Acta*, 1997, **36**, 262–268.
19 M. S. Sacks, *J. Elast.*, 2000, **61**, 199–246.
20 B. A. Roeder, K. Kokini, J. E. Sturgis, J. P. Robinson and S. L. Voytik-Harbin, *J. Biomech. Eng.*, 2002, **124**, 214–222.
21 C. Storm, J. J. Pastore, F. C. MacKintosh, T. C. Lubensky and P. A. Janmey, *Nature*, 2005, **435**, 191–194.
22 S. Motte and L. J. Kaufman, *Biopolymers*, 2013, **99**, 35–46.
23 P. H. J. Kouwer, M. Koepf, V. A. A. Le Sage, M. Jaspers, A. M. van Buul, Z. H. Eksteen-Akeroyd, T. Woltinge, E. Schwartz, H. J. Kitto and R. Hoogenboom, *et al.*, *Nature*, 2013, **493**, 651–655.
24 C. P. Broedersz and F. C. MacKintosh, *Rev. Mod. Phys.*, 2014, **86**, 995.
25 Q. Wen, A. Basu, P. A. Janmey and A. G. Yodh, *Soft Matter*, 2012, **8**, 8039–8049.
26 H. Kang, Q. Wen, P. A. Janmey, J. X. Tang, E. Conti and F. C. MacKintosh, *J. Phys. Chem. B*, 2009, **113**, 3799–3805.
27 E. Conti and F. C. MacKintosh, *Phys. Rev. Lett.*, 2009, **102**, 088102.
28 A. Kabla and L. Mahadevan, *J. R. Soc., Interface*, 2007, **4**, 99–106.
29 P. R. Onck, T. Koeman, T. Van Dillen and E. Van der Giessen, *Phys. Rev. Lett.*, 2005, **95**, 178102.
30 I. K. Piechocka, A. S. G. van Oosten, R. G. M. Breuls and G. H. Koenderink, *Biomacromolecules*, 2011, **12**, 2797–2805.
31 A. J. Licup, S. Münster, A. Sharma, M. Sheinman, L. M. Jawerth, B. Fabry, D. A. Weitz and F. C. MacKintosh, *Proc. Natl. Acad. Sci. U. S. A.*, 2015, **112**, 9573–9578.
32 A. Sharma, A. J. Licup, K. A. Jansen, R. Rens, M. Sheinman, G. H. Koenderink and F. C. MacKintosh, *Nat. Phys.*, 2016, DOI: 10.1038/nphys3628.
33 R. H. Pritchard, Y. Y. S. Huang and E. M. Terentjev, *Soft Matter*, 2014, **10**, 1864–1884.
34 F. C. MacKintosh, J. Käs and P. A. Janmey, *Phys. Rev. Lett.*, 1995, **75**, 4425.
35 D. C. Morse, *Macromolecules*, 1998, **31**, 7030–7043.
36 D. A. Head, A. J. Levine and F. C. MacKintosh, *Phys. Rev. Lett.*, 2003, **91**, 108102.
37 J. Wilhelm and E. Frey, *Phys. Rev. Lett.*, 2003, **91**, 108103.
38 M. Das, F. C. MacKintosh and A. J. Levine, *Phys. Rev. Lett.*, 2007, **99**, 038101.
39 C. Heussinger and E. Frey, *Phys. Rev. E: Stat., Nonlinear, Soft Matter Phys.*, 2007, **75**, 011917.
40 X. Mao, O. Stenull and T. C. Lubensky, *Phys. Rev. E: Stat., Nonlinear, Soft Matter Phys.*, 2013, **87**, 042602.
41 X. Mao, O. Stenull and T. C. Lubensky, *Phys. Rev. E: Stat., Nonlinear, Soft Matter Phys.*, 2013, **87**, 042601.
42 C. Heussinger, B. Schaefer and E. Frey, *Phys. Rev. E: Stat., Nonlinear, Soft Matter Phys.*, 2007, **76**, 031906.
43 H. Hatami-Marbini and M. R. Mofrad, *Cellular and Biomolecular Mechanics and Mechanobiology*, Springer, 2011, pp. 3–27.
44 A. M. Stein, D. A. Vader, D. A. Weitz and L. M. Sander, *Complexity*, 2011, **16**, 22–28.
45 A. S. G. van Oosten, M. Vahabi, A. J. Licup, A. Sharma, P. A. Galie, F. C. MacKintosh and P. A. Janmey, *Sci. Rep.*, 2016, **6**, 19270.
46 K. Comley and N. Fleck, *Int. J. Impact Eng.*, 2012, **46**, 1–10.
47 W. Bonfield and M. D. Grynpas, *Nature*, 1977, **270**, 453–454.
48 D. M. Elliott and L. A. Setton, *J. Biomech. Eng.*, 2001, **123**, 256–263.
49 P. D. Soden and I. Kershaw, *Med. Biol. Eng.*, 1974, **12**, 510–518.
50 C. Lally, A. J. Reid and P. J. Prendergast, *Ann. Biomed. Eng.*, 2004, **32**, 1355–1364.
51 L. A. Mihai, L. Chin, P. A. Janmey and A. Goriely, *J. R. Soc., Interface*, 2015, **12**, 20150486.
52 M. Perepelyuk, L. Chin, X. Cao, A. van Oosten, V. B. Shenoy, P. A. Janmey and R. G. Wells, *PLoS One*, 2016, **11**, 1–18.
53 K. Pogoda, L. Chin, P. C. Georges, F. J. Byfield, R. Bucki, R. Kim, M. Weaver, R. G. Wells, C. Marcinkiewicz and P. A. Janmey, *New J. Phys.*, 2014, **16**, 075002.
54 H.-C. Wu and R.-F. Yao, *J. Biomech.*, 1976, **9**, 1–7.
55 O. A. Shergold, N. A. Fleck and D. Radford, *Int. J. Impact Eng.*, 2006, **32**, 1384–1402.
56 R. W. Ogden, *Proc. R. Soc. London, Ser. A*, 1972, 565–584.
57 S. B. Lindström, D. A. Vader, A. Kulachenko and D. A. Weitz, *Phys. Rev. E: Stat., Nonlinear, Soft Matter Phys.*, 2010, **82**, 051905.
58 C. Robertson, K. Ikemura, T. B. Krasieva and S. C. George, *Biomaterials*, 2013, **34**, 6127–6132.
59 Y.-c. Fung, *A first course in continuum mechanics*, Prentice Hall, 2nd edn, 1977.
60 M. Destrade, Y. Liu, J. G. Murphy and G. S. Kassab, *J. Theor. Biol.*, 2012, **303**, 93–97.
61 K. A. Jansen, R. G. Bacabac, I. K. Piechocka and G. H. Koenderink, *Biophys. J.*, 2013, **105**, 2240–2251.
62 P. Kollmannsberger, C. T. Mierke and B. Fabry, *Soft Matter*, 2011, **7**, 3127–3132.
63 D. Mizuno, C. Tardin, C. F. Schmidt and F. C. MacKintosh, *Science*, 2007, **315**, 370–373.
64 C. J. Jen and L. V. McIntire, *Cell Motil.*, 1982, **2**, 445–455.
65 S. Q. Liu and Y. C. Fung, *J. Biomech. Eng.*, 1989, **111**, 325–335.
66 M. K. Hong, J. Vossoughi, G. S. Mintz, R. D. Kauffman, R. F. Hoyt, J. F. Cornhill, E. E. Herderick, M. B. Leon and J. M. Hoeg, *Arterioscler., Thromb., Vasc. Biol.*, 1997, **17**, 2209–2217.

67 F. C. MacKintosh and A. J. Levine, *Phys. Rev. Lett.*, 2008, **100**, 018104.
68 P. M. Bendix, G. H. Koenderink, D. Cuvelier, Z. Dogic, B. N. Koeleman, W. M. Brieher, C. M. Field, L. Mahadevan and D. A. Weitz, *Biophys. J.*, 2008, **94**, 3126–3136.
69 C. P. Broedersz and F. C. MacKintosh, *Soft Matter*, 2011, **7**, 3186–3191.
70 C. P. Broedersz, M. Sheinman and F. C. MacKintosh, *Phys. Rev. Lett.*, 2012, **108**, 078102.
71 J. C. Maxwell, *Philos. Mag. J. Sci.*, 1864, **27**, 294–299.
72 M. F. Thorpe, *J. Non-Cryst. Solids*, 1983, **57**, 355–370.
73 M. Sheinman, C. P. Broedersz and F. C. MacKintosh, *Phys. Rev. Lett.*, 2012, **109**, 238101.
74 S. Alexander, *Phys. Rep.*, 1998, **296**, 65–236.
75 M. Dennison, M. Sheinman, C. Storm and F. C. MacKintosh, *Phys. Rev. Lett.*, 2013, **111**, 095503.
76 A. W. Lees and S. F. Edwards, *J. Phys. C: Solid State Phys.*, 1972, **5**, 1921.
77 M. Das, D. A. Quint and J. M. Schwarz, *PLoS One*, 2012, **7**, e35939.
78 R. Rens, M. Vahabi, A. J. Licup, F. C. MacKintosh and A. Sharma, *J. Phys. Chem. B*, 2016, DOI: 10.1021/acs.jpcb.6b00259.
79 A. J. Licup, A. Sharma and F. C. MacKintosh, *Phys. Rev. E: Stat., Nonlinear, Soft Matter Phys.*, 2016, **93**, 012407.
80 L. Landau and E. Lifshitz, *Course of Theoretical Physics*, Theory of Elasticity, Oxford, 1970, vol. 7.
81 W. H. Press, S. A. Teukolsky, W. T. Vetterling and B. P. Flannery, *Numerical recipes in C*, Cambridge University Press Cambridge, 1996, vol. 2.
82 A. E. Brown, R. I. Litvinov, D. E. Discher, P. K. Purohit and J. W. Weisel, *Science*, 2009, **325**, 741–744.
83 I. K. Piechocka, K. A. Jansen, C. P. Broedersz, N. A. Kurniawan, F. C. MacKintosh and G. H. Koenderink, *Soft Matter*, 2016, **12**, 2145–2156.
84 Z. Qin and M. J. Buehler, *Phys. Rev. Lett.*, 2010, **104**, 198304.
85 A. Zhmurov, O. Kononova, R. I. Litvinov, R. I. Dima, V. Barsegov and J. W. Weisel, *J. Am. Chem. Soc.*, 2012, **134**, 20396–20402.
86 K. M. Heidemann, A. Sharma, F. Rehfeldt, C. F. Schmidt and M. Wardetzky, *Soft Matter*, 2015, **11**, 343–354.
87 P. A. Janmey, M. E. McCormick, S. Rammensee, J. L. Leight, P. C. Georges and F. C. MacKintosh, *Nat. Mater.*, 2007, **6**, 48–51.
88 J. H. Poynting, *Proc. R. Soc. London, Ser. A*, 1909, **82**, 546–559.
89 J. H. Poynting, *Proc. R. Soc. London, Ser. A*, 1912, 534–561.